Optimization of Composite Wing Structure with Static, Buckling, and Flutter Constraints using the Finite Element Method

Muhammad Kusni[*], *H. Syamsudin, L. Gunawan, Bambang Kismono Hadi*
Faculty of Mechanical and Aerospace Engineering ITB, INDONESIA
[*]*kusni@ae.itb.ac.id*

Seno Darmanto
Faculty of Mechanical Engineering, Diponegoro University, INDONESIA

M. Akhsin Muflikhun
Faculty of Mechanical Engineering, Gadjah Mada University, INDONESIA

Martina Widiramdhani
Garuda Maintenance Facility GMF, Soekarno Hatta (CGK), INDONESIA

ABSTRACT

In airplane structural design, creating a strong yet lightweight structure is crucial. During the preliminary design phase, structural sizing optimization is necessary to achieve an efficient and lightweight structure that meets safety standards. Composite materials offer a high strength-to-weight ratio, enabling a lighter structure without compromising strength. This work focuses on optimizing composite structure wings by considering laminae thicknesses as design variables and minimizing structure weight as the objective, using the gradient-based method. The optimization constraints include the Tsai-Hill criterion, buckling factor, and flutter speed to ensure the structure's safety against static load, buckling phenomena, and flutter phenomena. The optimization results indicate that the buckling factor is the most critical constraint, carrying the highest weight. The weight of the wing structure decreased by 53% and 79% after optimizing with static and flutter constraints, respectively. Despite minimal changes in weight after optimizing with the buckling constraint, the structure now meets the buckling safety criteria and is safe from buckling.

ISSN 1823-5514, eISSN 2550-164X
© 2024 College of Engineering,
Universiti Teknologi MARA (UiTM), Malaysia.
https://doi.org/10.24191/jmeche.v21i3.27358

Received for review: 2022-10-13
Accepted for publication: 2023-12-08
Published: 2024-09-15

Keywords: *Optimization; Composite; Static; Buckling; Flutter*

Introduction

In aircraft structure design, it is crucial to prioritize strength and weight reduction. The weight of an aircraft impacts its performance, manufacturing costs, and operational expenses. Therefore, optimizing the structure is essential to creating a lightweight design that adheres to safety standards.

Vanderplaats [1] pioneered structural optimization and made key observations about its future. Ganguli [2] discussed the extensive utilization of composite materials in aircraft structures. Khot et al. [3] published one of the initial papers on composite optimization. Their work focused on an efficient optimization method based on strain energy distribution and numerical search techniques to minimize composite structure weight. Starnes and Haftka [4] demonstrated the advantages of composite materials over aluminum designs.

Weisshaar [5] and Shirk [6] studied how composite tailoring affects divergence, lift effectiveness, and center-of-pressure location, demonstrating the adaptability of composite materials to aeroelastic constraints. Eastep et al. [7] conducted an optimization study for composite wing design using the Multidisciplinary Design Optimization (MDO) code called ASTROS.

Hadi et al. [8] and [9] used optimization techniques and the finite element method to handle static, buckling, and flutter constraints in designing a composite wing for a High Aspect Ratio HALE aircraft. This paper focuses on the design of a high aspect ratio wing for a HALE UAV, intended for high-altitude and long-duration flights, using the Global Hawk RQ-4A as a test case.

Static strength analysis using Tsai-Wu failure criteria is conducted, comparing carbon/epoxy T300/5208 with aluminum 2024-T3. Two laminate configurations are considered: (0°/0°/+45°/-45°)s and quasi-isotropic (0°/+45°/-45°/90°)s. The goal is to achieve a lightweight design that meets strength requirements. The finite element method is employed using NASTRAN software. Results show that the (0°/0°/+45°/-45°)s configuration is 30% lighter than quasi-isotropic and 60% lighter than the aluminum wing.

Wanga et al. [10] conducted research on optimizing wing-box structures using variable-angle-tow composite fibers to minimize mass and enhance performance against buckling and aeroelastic failures. Feil et al. [11] presented a cross-sectional aeroelastic analysis and structural optimization tool for slender composite structures.

Yang et al. [12] performed structural optimization by combining the Automated Finite Element Modeling (AFEM) technique with the Ground Structure Approach (GSA) for aircraft wing geometry, considering fuel tanks, landing gear, and control surface arrangements. Jonsson et al. [13] discussed flutter analysis as a constraint in multidisciplinary design optimization, while Fernandez-Escudero et al. [14] compared numerical methods for unsteady

aerodynamics and nonlinear aeroelasticity, including low, medium, and high fidelity models.

This paper represents a continuation of the previous work by Kusni et al. [15], which focused on sensitivity analysis and structural optimization using aluminum material. In this study, we use composite materials and mathematical optimization to determine the optimal thickness of wing components, considering static, buckling, and flutter constraints. The optimization is performed using a solver with a gradient-based method.

Firstly, we analyze the structural strength of the wing under static and buckling loads and assess the flutter speed of the initial wing design. Subsequently, we present the modifications made to the wing structure components after optimization, while considering limitations such as Tsai Hill failure, buckling, and flutter speed criteria. Finally, we showcase the optimal size and minimum weight of the wing component structure that satisfies all these constraints, including static, buckling, and flutter requirements.

This paper provides a comprehensive exploration of modern aircraft design optimization, specifically focusing on the use of composite materials and considering multiple constraints, such as static, buckling, and aeroelasticity, in comparison to prior research. By employing finite element analysis, the proposed methodology can be directly applied to real-world aircraft structures. Additionally, this study presents a comparative analysis of the weight of aircraft wing structures constructed using aluminum and carbon composite materials, a facet that has not been thoroughly investigated in previous literature.

The methodology employed in this study follows a systematic approach. Initially, a geometric model and wing support model were created using MSC Patran. Subsequently, static, buckling, and flutter analyses were conducted on the initial configuration to assess its performance. Optimization was then carried out with the objective of minimizing the weight of the structure. The design variables encompassed the geometric dimensions of the structure of the composite material. Static, buckling, and flutter failures were established as design constraints. The resulting dimensions of the structure were determined to be the most optimal by the optimization solver.

However, since the three constraints were optimized individually, it is necessary to re-evaluate whether the structure dimensions or the number of composite layers satisfy all the specified constraints. The optimization process of composite wing structures with static, buckling, and flutter constraints using the finite element method can be described in the flowchart presented in Figure 1.

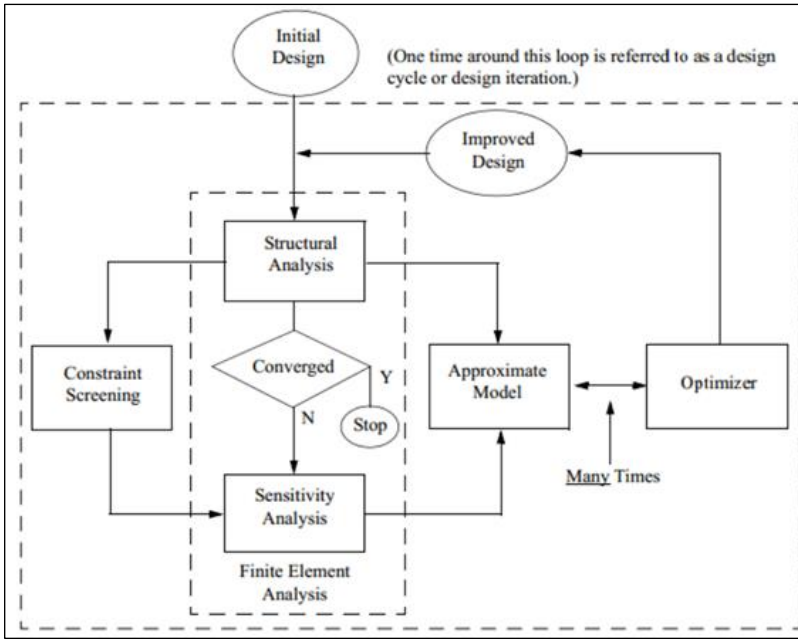

Figure 1: The optimization process of composite wing structures with static, buckling, and flutter constraints using the finite element method

Finite Element Modelling and Component Optimization

Finite element modeling

The wing structure is modeled as a plate structure consisting of skin, rib, front spar, and rear spar. Each structural member is a plate component built on CATIA V5 Software as shown in Figure 2(a).

Structure modeling and area division

The skin consists of 22 plates, which are then grouped into 7 groups as shown in Figure 2(b). The direction of the wingspan is the x-axis, and the chord direction of the wing is the y-axis.

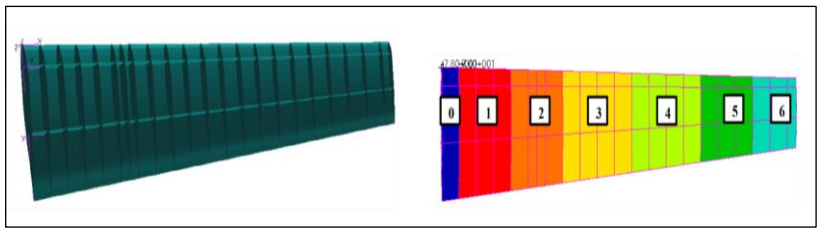

(a) (b)

Figure 2: (a) Structural geometry, and (b) division of skin area

Ribs consist of 23 plates, which are then grouped into 6 groups as shown in Figure 3(a). The chord direction of the wing is the x-axis, and the vertical of the wing is the y-axis.

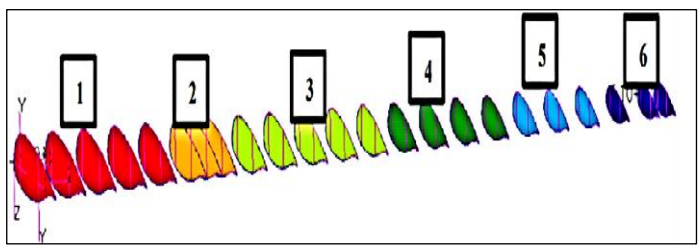

(a)

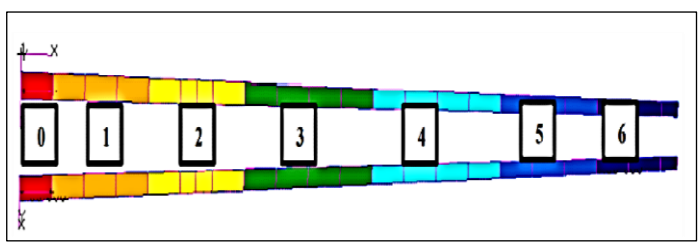

(b)

Figure 3: (a) Division of ribs area, and (b) division of spar area

The front spar and rear spar consist of 22 plates, the same as the skin and spar, which are then grouped into 7 groups as shown in Figure 3(b). The direction of the wingspan is the x-axis, and the vertical direction is the y-axis.

A critical stage in finite element modeling is meshing, where mostly quad elements are used, along with a small proportion of triad elements. In this study, the element size for the structure was set to 20 mm. Convergence tests

demonstrated that this element size was valid, with changes in the results within a range of 7.38% when compared to an element size of 50 mm.

In the finite element model, the skewness value, or Jacobian ratio, is a measure of the quality of the elements used in the mesh. The skewness value, or Jacobian ratio, is calculated for each finite element within the mesh. It's important to note that the acceptable limits for skewness values or Jacobian ratios depend on the specific analysis being conducted, the element types used, and the software guidelines. In general, lower skewness values and Jacobian ratios closer to 1 are desired for accurate and stable simulations. Higher skewness values or significantly deviating Jacobian ratios may indicate elemental distortion or deformation.

In the FEM model, the skewness value, or Jacobian ratio, is typically determined based on the element formulation and the nodal coordinates. The specific method used to calculate skewness or Jacobian ratio depends on the element type and formulation being used in the FEM model. For the cases mentioned in the paper, here are the outputs:

i. QUAD4 element ID 4010 produced the smallest skew angle of 19.48 (tolerance = 30.00).
ii. QUAD4 element ID 3490 produced the smallest interior angle of 16.46 (tolerance = 30.00).
iii. QUAD4 element ID 3170 produced the largest interior angle of 165.42 (tolerance = 150.00).

Properties and materials of structural components

All structural members were modeled as a composite plate having a symmetrical arrangement [0°k/45°l/-45°l/90°n] with a lamina thickness of 45° and -45° made the same.

Table 1: Graphite/epoxy material properties

Material properties GY70/934 Graphite/Epoxy					
Density	1590	Kg/m^3	Tension stress limit II	9.85E+08	Pa
Elastic modulus	2.94E+11	Pa	Tension stress limit 22	2.90E+07	Pa
Elastic 22	6.40E+09	Pa	Compress stress limit	6.90E+08	Pa
Poison Ration12	0.23	Pa	Compress stress limit 22	9.80E+07	Pa
Shear modulus 12	4.90E+09	Pa	Shear stress limit	4.90E+07	Pa

Table 1 presents the material properties of the GY70/934 Graphite/Epoxy composite. GY 70/934 is a composite material commonly used in aerospace and structural applications. It combines epoxy resin and glass fibers to provide several key properties:

i. Strong and maintains structural integrity under high loads.
ii. Highly rigid, resisting deformation under applied forces.
iii. Lightweight with a favorable strength-to-weight ratio due to glass fiber reinforcement.
iv. Durable with resistance to moisture and chemicals.
v. Versatile for manufacturing, including molding, pultrusion, and filament winding.

Overall, GY 70/934 is a composite material that combines the favorable properties of epoxy resin and glass fibers. Its strength, stiffness, lightweight nature, durability, and manufacturing versatility make it suitable for a wide range of high-performance applications.

The initial thickness of each component varies depending on its location. Components located in the root area have a greater thickness than those located in the wingtip area. The initial thickness for each component is shown in Table 2. The initial thickness is obtained from the initial design of the structure.

Table 2: Initial laminate thickness of each component

		Number of layers per area									**Number of layers per area**						
		0	**1**	**2**	**3**	**4**	**5**	**6**			**0**	**1**	**2**	**3**	**4**	**5**	**6**
Skin	0°	8	7	6	6	5	4	2	Rib	0°	-	4	4	3	3	2	2
	45°	8	7	6	6	5	4	2		45°	-	4	4	3	3	2	2
	135°	8	7	6	6	5	4	2		135°	-	4	4	3	3	2	2
	90°	8	7	6	6	5	4	2		90°	-	4	4	3	3	2	2
	Total	64	56	48	18	40	32	16		Total	-	32	32	24	24	16	16
Front spar	0°	8	7	6	4	3	2	1	Rear spar	0°	8	7	6	4	3	2	1
	45°	8	7	6	4	3	2	1		45°	8	7	6	4	3	2	1
	135°	8	7	6	4	3	2	1		135°	8	7	6	4	3	2	1
	90°	8	7	6	4	3	2	1		90°	8	7	6	4	3	2	1
	Total	64	56	48	32	24	16	8		Total	64	56	48	32	24	16	8

Boundary condition

The wing structure is given a fixed boundary condition at the root, with the assumption that it is given a joint on the spar and part of the skin. Figure 4 shows the boundary conditions. There is no translational and rotational movement in the x, y, or z directions.

Loading

The maximum load experienced by the aircraft is used for calculating the static strength. The aircraft is designed to be maneuverable at a load factor of 2.5 g. The maximum load (L) for the half wing is 170.4 kN. The total force is distributed on each skin plate with a Schrenk distribution.

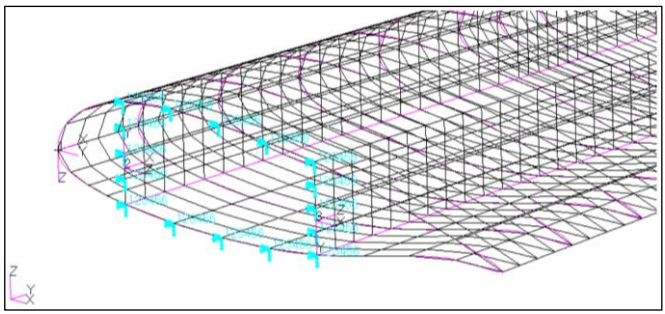

Figure 4: Boundary conditions at the wing root

Optimization Modeling

Design objective

The purpose of the optimization process in this work is to get the lightest possible weight of the structure without going over the set limits. Therefore, the design objective is to reduce the weight of the structure.

Design variable

The design variable used is the thickness of the composite material for each lamina. The thinnest laminate layer for Graphite and Epoxy materials is usually 0.125 mm, so the minimum limit for each lamina is 1 layer (0.125 mm). The minimum total thickness of 8 layers is 1 mm, and the maximum thickness for one layer of the lamina is 2.5 mm (20 layers). The maximum total thickness is 2 cm (160 layers). Optimization is carried out continuously, with discrete optimization in the final design after continuous optimization is completed.

Constraints

There are 3 constraints set in the optimization in the case in this paper, namely the static, buckling, and flutter speed constraints.

Static constraints

The structure is required to be strong enough to accept static loads. It is proven by using the Tsai-Hill failure criteria with Equation (1). The Tsai-Hill failure index must not exceed or be equal to 1 to be considered safe.

$$\left(\frac{\sigma_1}{X}\right)^2 - \frac{\sigma_1\sigma_2}{X^2} + \left(\frac{\sigma_2}{X}\right) + \left(\frac{\tau_{12}}{S}\right)^2 \leq 1 \qquad (1)$$

Buckling constraint

The structure must not exceed the critical buckling load. With Pcr is the

critical buckling load, and P_{app} is the load received by the structure. The Buckling Factor is shown in Equation (2).

$$BF = \left(\frac{P_{cr}}{P_{app}}\right) \geq 1 \tag{2}$$

Flutter speed constraint

Flutter occurs when the structure is no longer able to dampen the vibrations that occur (positive aerodynamic damping). The flutter speed that is used as a limitation in this paper is 500 m/s. At this speed, the structural damping + aerodynamic damping cannot be negative. To make this damping limit, we cannot simply enter a 0.0 limit on damping, because MSC Nastran will face difficulties because there will be a division by 0. To prevent this problem, the form of the damping flutter constraint becomes;

$$R2 = \frac{\gamma - OFFSET}{GFACT} \tag{3}$$

with $R2$ as a second-level response and γ as a damping structure, the $OFFSET$ used is usually 0.03, and $GFACT$ scaling factor is 0.1.

Analysis and Optimization Results

Optimization with static stress constraints

Structural thickness optimization results (static constraint)

From the results obtained, it can be concluded that, in general, the lamina with the fiber direction of 0° is always thicker than the lamina in the other direction. The lamina in the 90° direction always has a minimum thickness. This is because the load and boundary conditions given to this wing make the wing receive the greatest tensile and compressive stress in the x-direction (0°), so the required strength in this direction is greater as well.

Figure 5 shows the thickness of the laminate for each area of the front spar. The result after optimization is generally smaller than the initial thickness before optimization, indicating that the optimization process has succeeded in reducing the thickness of the structure.

Figures 6, 7, and 8 show the total thickness of the rear spar, skin, and rib components. The final thickness becomes smaller than the initial thickness. In every figure, there is always an incline in the last iteration. This is because the last iteration process is a discrete optimization process. The first optimization process to the 6th is a continuous optimization process, then discrete optimization is carried out at the end of the optimization so that the thickness is an integer multiple of 0.125 mm.

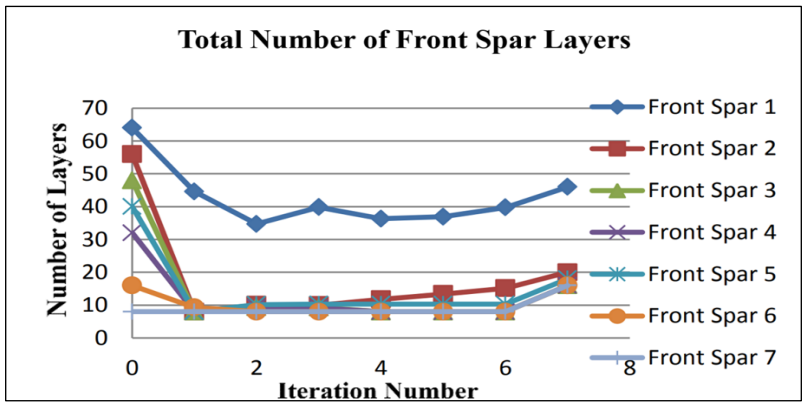

Figure 5: Number of front spar layers

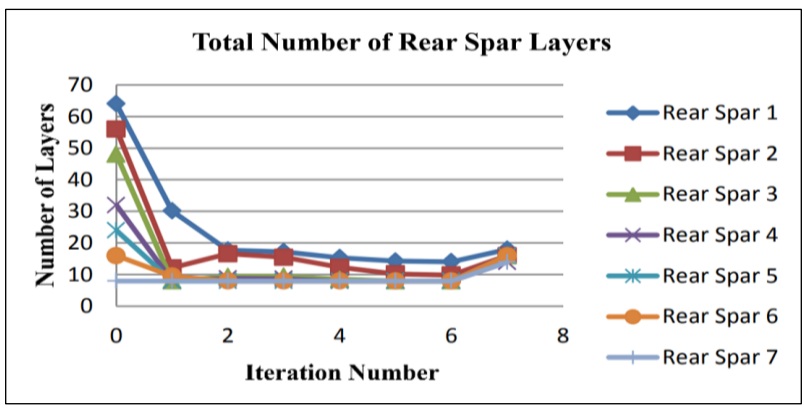

Figure 6: Number of rear spar layers

The skin and front spar possess the highest thickness among the other components. This is attributed to their role in effectively withstanding the bending moment experienced by the wing. The load applied to the wing is only a static aerodynamic load that is placed on the top and bottom skin nodes of the wing.

Structural weight optimization results (static constraint)

Figure 9 shows the weight comparison of the results of the optimization of the structure with composites and structures that use aluminum. After optimization, the composite experienced a considerable weight reduction of almost 70% in the 6th iteration as shown in Table 3, but after the discretization process, it became 53%. When compared with aluminum, composite materials

are superior in terms of weight because the structure with composite materials is lighter than aluminum by up to 22%.

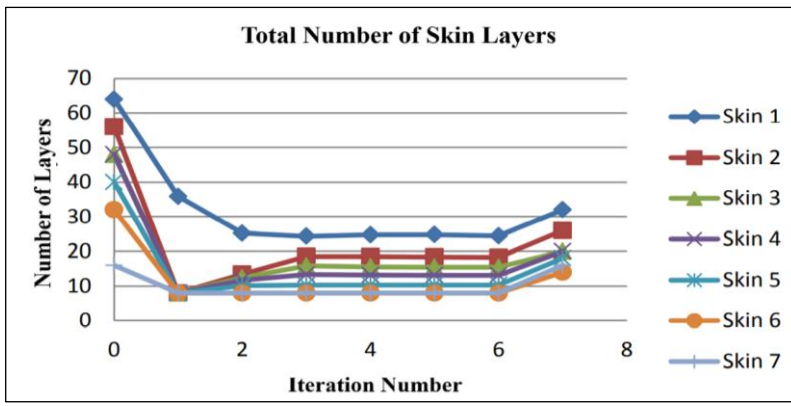

Figure 7: Number of skin layers

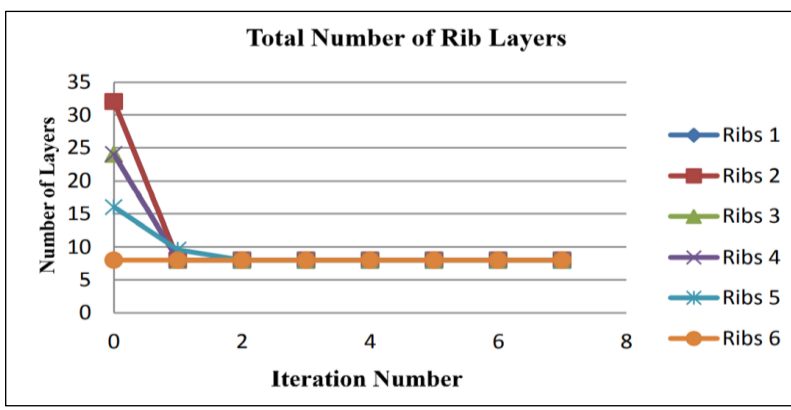

Figure 8: Number of rib layers

Comparison after and before optimization (static constraints)

The wing structure has been successfully optimized, and the static stress constraint received by the wing should not exceed the limits of the Tsai Hill criteria. The initial weight of the structure is 485 kg after being optimized to 228 kg, or reduced by 53% from the initial weight analyzed. The margin of safety of the structure became more optimal, which was initially 0.39 after being optimized to 0.12.

The maximum stress received by the structure was initially 196 Mpa, but after optimization, the structure was still able to withstand stresses of up to

418 MPa, while Aluminum was only able to withstand stresses of up to 328 MPa. Table 4 shows the comparison before and after optimization with static constraints.

Table 3: Weight comparison

Iteration	Al (kg)	Composite (kg)
0	585	485
1	375	115
2	317	134
3	296	149
4	293	148
5	293	148
6	293	147
7	-	228

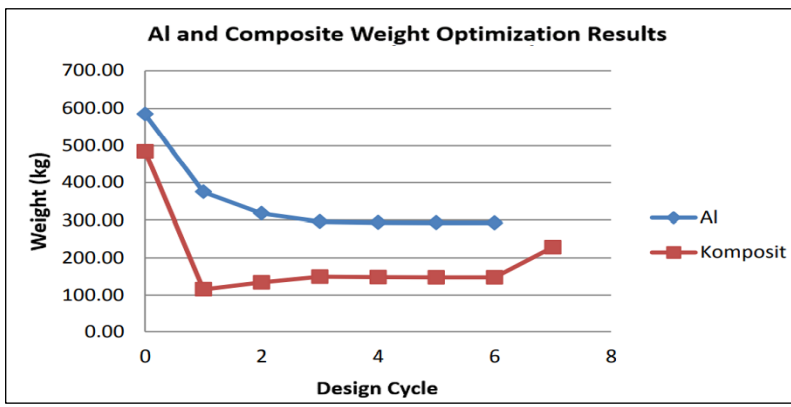

Figure 9: Structural weight optimization results (static constraints)

Table 4: Comparison before and after optimization (static constraints)

	Initial	Final
Weight	485 kg	228 kg
Margin of safety	0.39	0.12
Maximum stress	196 MPa	418 MPa
Tsai-Hill Failure Index	0.52	0.8
Aluminium Maximum Stress	292 MPa	328 MPa

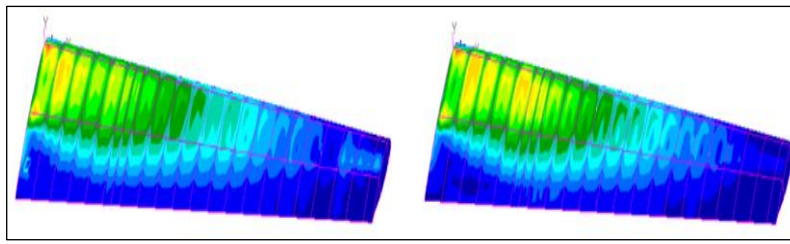

(a) (b)

Figure 10: Stress distribution; (a) before, (b) after optimization

Optimization with buckling factor constraints

In contrast to the static stress, which is affected by matrix A on the laminated composite stiffness matrix (ABD matrix), the buckling calculation based on the buckling equation actually depends on the value of the D matrix as the flexural stiffness matrix. The stacking sequence affects the value of the D matrix, which means that it also affects the value of the buckling factor; therefore, in this paper, a parametric study with three sequences is carried out. The first arrangement is the basic arrangement used in optimization with static stress limits, namely [0°/45°/-45°/90°], the second arrangement is [45°/-45°/90°/0°], and the third arrangement is [90°/45°/-45°/0°].

Optimization results of structure thickness (buckling constraint)

Optimization with static stress constraints resulted in the maximum thickness of the fiber at an angle of 0°, but optimization with buckling constraints made the 90° and 45° angles experience significant thickening. Table 5 shows the direction in which fiber is the thickest in the skin component. The wing structural components observed here are only skin components because these components are the most susceptible to buckling.

In the first arrangement, in general, the fiber direction of 90° is the thickest lamina. Likewise, in the second arrangement, generally, the fiber direction is 90° and the thickest. However, in the third arrangement, it is precisely the 0° fiber direction that has the thickest lamina.

If we look at the number of layers in other parts besides the skin, usually the 45° fiber direction has the highest number of layers. In the case of pure compression, usually the 45° fiber direction is the most decisive because this fiber direction makes the D66 component in the D matrix larger, but in the skin, what happens is not pure compression.

The loading that occurs and the shape of the skin are not completely straight, making the forces that occur on the skin complex so that the thickest angle is no longer 45°.

Table 5: Number of skin component layers (buckling constraint)

	0°/45°/135°/90°	**0°/45°/135°/90°**	**0°/45°/135°/90°**
0°/45°/135°/90°	**12**	2	**13**
	7	10	11
	6	**14**	9
0°/45°/135°/90°	8	5	**16**
	9	9	11
	9	**12**	5
0°/45°/135°/90°	**11**	2	**10**
	4	7	10
	9	**11**	4
90°/45°/135°/90°	3	2	**16**
	7	6	6
	10	**9**	2
0°/45°/135°/90°	3	1	**7**
	4	4	6
	9	**7**	5
0°/45°/135°/90°	2	1	**4**
	3	3	4
	3	**4**	2
0°/45°/135°/90°	1	**2**	**2**
	2	1	2
	2	1	1

Optimization result of structure weight (buckling constraint)

Table 6 and Figure 11 show a comparison of the weight of the wing optimization results using composites and aluminum. There is a very significant difference between composite wings and aluminum wings. The aluminum wings increased by 62% of their initial weight to 946 kg. The increase in weight is due to the initial sizing of the wing having a very small buckling factor value of only 0.2. Therefore, a significant increase in thickness was carried out so that the buckling factor value exceeded 1 (the safe limit). In the case of composite wings, there is not too much difference. Composite wings with the first arrangement are up to 51% lighter than aluminum wings. From Table 6, it can be concluded that the composite with the first arrangement is better than the second and third arrangements with buckling constraints.

Table 6: Weight comparison of optimization results (buckling constraint)

	Initial	**Final**
[0/450-45/90]	485 kg	484 kg
[45/-45/90/0]	485 kg	521 kg
[90/45/-45/0]	485 kg	566 kg
Al 2024-T3	585 kg	946 kg

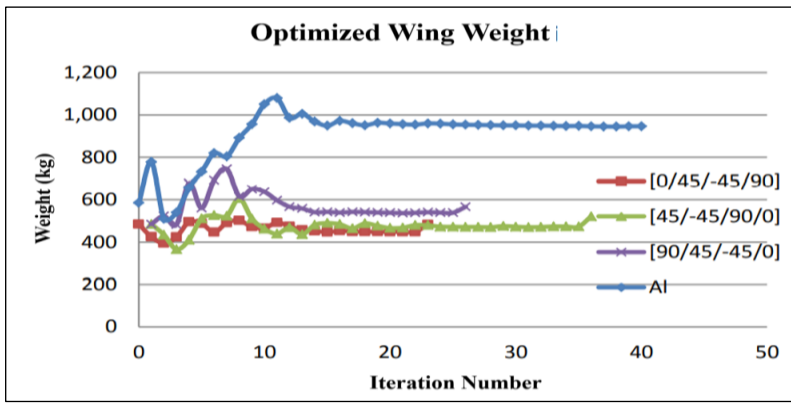

Figure 11: Comparison of wing weight from optimization results

Comparison after and before optimization (buckling constraint)

From the weight data before and after optimization as in Table 7, the first laminate arrangement has the lightest weight after being optimized. Therefore, the final configuration used is a composite with the first laminate arrangement.

Table 7: Comparison of before and after optimization (buckling constraints)

	Initial	**Final**
Weight	485 kg	484 kg
Buckling factor	0.6561	1.0892
Maximum static stress	189 MPa	191 MPa
Buckling critical stress	124 MPa	208 MPa
Tsai-Hill failure index	0.404	0.356

Wing weight after optimization is almost not reduced, but the value of the buckling factor has increased up to 65% from its initial value. Although the initial structure is safe from static stress limits, it does not meet the buckling criteria. The load received by the wing is above the critical buckling load, so buckling still occurs. After optimization, the structure is said to be safe from the buckling phenomenon because the load received is below the critical

buckling load. After optimizing buckling, it is necessary to ascertain whether the structure is also safe from static stress constraints. The Tsai-Hill failure index after optimization is 0.356. Thus, the structure is still safe against the static stresses that occur. Judging from the failure index, the structure becomes more inefficient, but an increase in weight is needed to meet the buckling constraint. Figures 12 and 13 show the buckling mode.

Optimization with flutter speed constraints.

The D matrix value affects the flutter speed similarly to the buckling constraint. No parametric studies were conducted for this constraint, assuming that the [0°/45°/-45°/90°] arrangement was superior to others.

Flutter velocity analysis of the initial structure

The composite structure used is the basic structure resulting from the initial design of the structure. It is known that the structure experiences the most critical flutter speed at sea level with a Mach number of 0.0, so the optimization is only carried out in that flight condition. The analysis was carried out using the MSC Nastran software with the PK method.

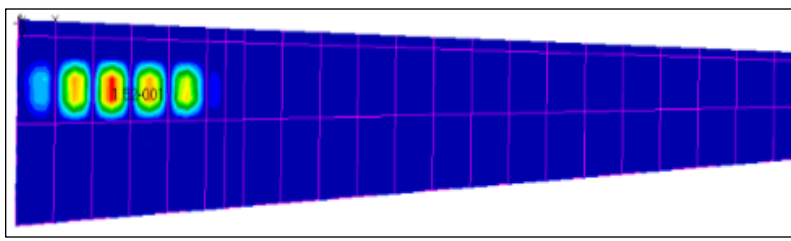

(a)

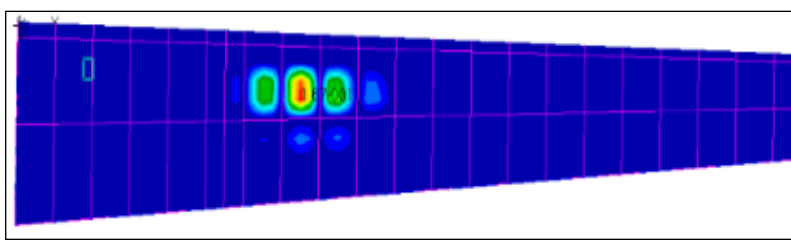

(b)

Figure 12: Buckling mode; (a) before, and (b) after optimization (lateral view)

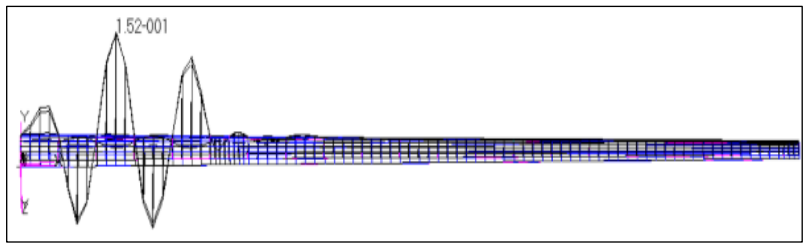

(a)

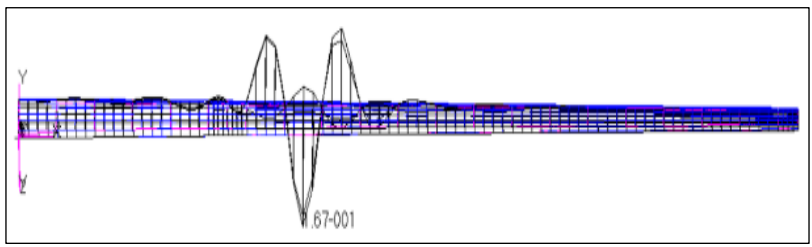

(b)

Figure 13: Buckling mode; (a) before, and (b) after optimization (longitudinal)

The results of the analysis show that the flutter speed value is 860 m/s, as shown by the damping-velocity graph, which exceeds 0.03 as the assumption of structural damping, as shown in Figure 14(a). The coupled modes are the 4th and 3rd modes, as shown in Figure 14(b). Figure 15 shows the coupled mode, namely: (a) the second bending mode at the 3rd frequency and (b) the first torsion mode at the 4th frequency.

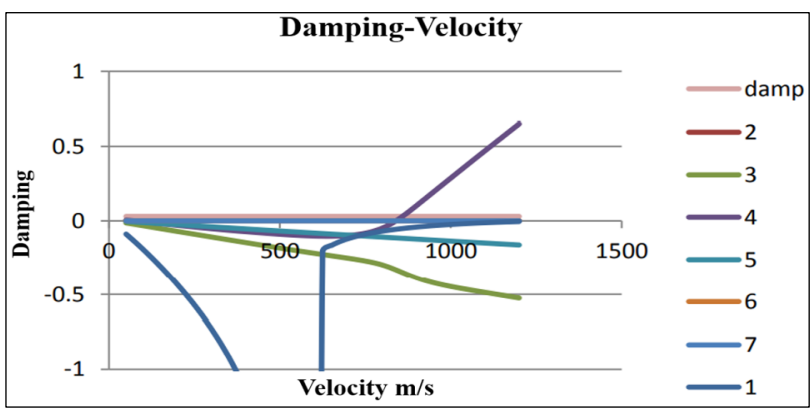

(a)

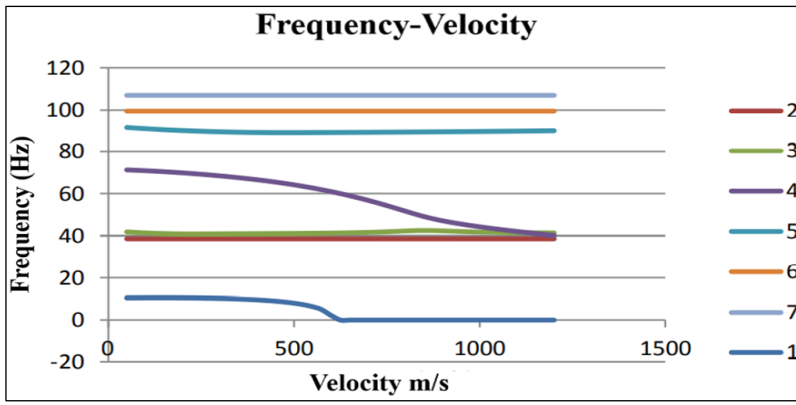

(b)

Figure 14: (a) Damping-velocity curve, and (b) frequency-velocity curve

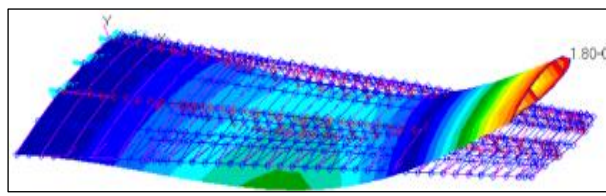

(a)

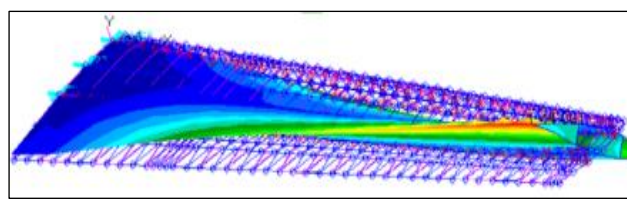

(b)

Figure 15: (a) 3rd frequency, and (b) 4th frequency

This initial analysis is very important to determine which mode is given the damping constraint. Because the flutter occurs in the 4th mode, the mode that is given a damping constraint is only the 4th mode at a speed of 500 m/s.

Optimization results of the thickness of the structure (flutter constraints)

After optimization with the damping constraint at a speed of 500 m/s, the results for the thickness of the structure are close to the minimum value. This is because the wing structure analyzed is quite rigid and has an aspect ratio that

is not too large, so it has a high flutter speed (safe for flutter).

Figures 16(a), 16(b), 17(a), and 17(b) show the thickness optimization history for each component. The optimization only consisted of 4 cycles, and the entire thickness of the components at the end of the optimization was only 0.125 mm, so the maximum thickness of each component was 1 mm. It should be noted that although the minimum thickness of the structure is still safe from flutter, in determining the thickness of the final structure, other constraints such as static stress and buckling have been optimized previously.

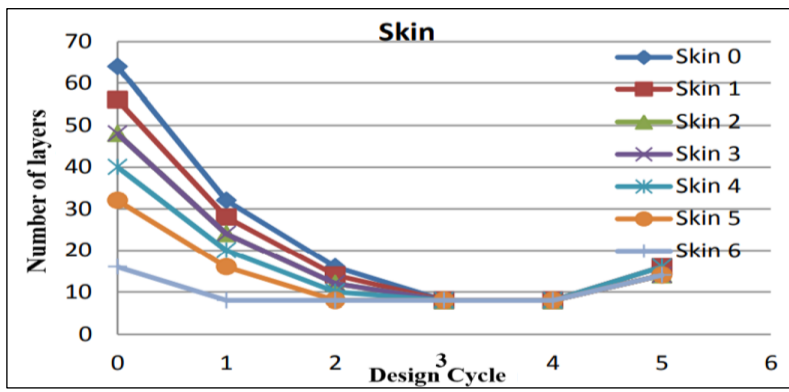

(a)

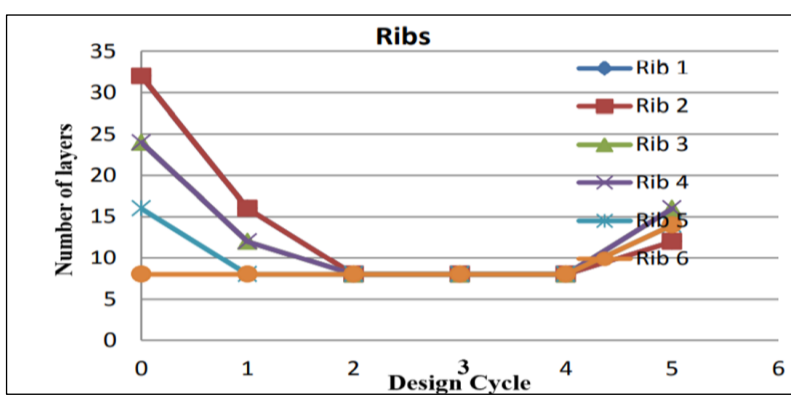

(b)

Figure 16: History of (a) skin layers, and (b) rib layers

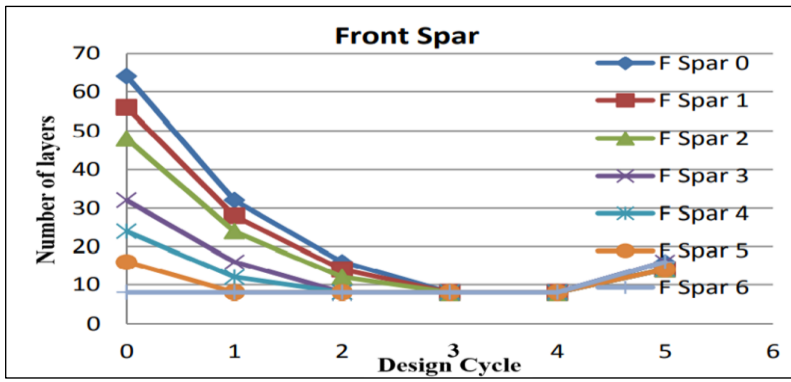

(a)

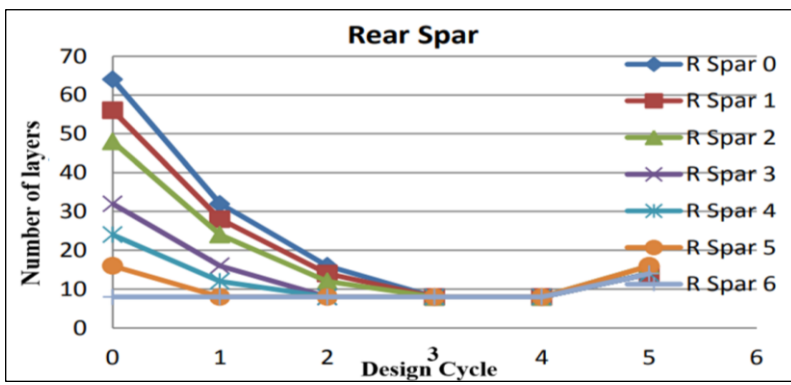

(b)

Figure 17: History of (a) front spar layers (b) rear spar layers

Optimization result of structure weight (flutter constraint)

Figure 18 shows the weight of the structure during optimization. Since the first cycle, the weight has been reduced by half and then continues to decrease until only 20% of it remains. The final total weight is the minimum structure weight of 96.6 kg.

Structure flutter analysis after optimization

A flutter analysis for the initial design was presented, which produced a flutter speed of 860 m/s. After optimization, the flutter speed drops to 550 m/s, meaning the flutter speed becomes more efficient with a flutter speed limit of 500 m/s. Before optimization, flutter occurs in the coupling mode between the first torsion mode and the second bending mode, or at the 4th and 3rd frequencies. After optimization, flutter occurs in the 5th mode (Figure 19) or

the first torque coupled to the 2nd bending mode or 3rd frequency.

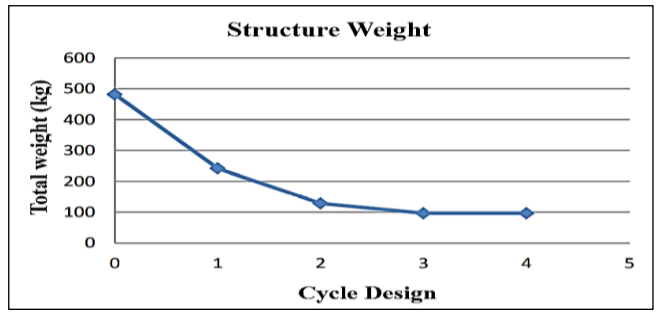

Figure: 18 Total weight optimization results

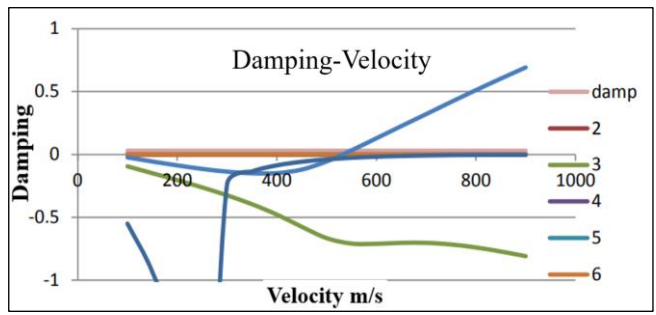

(a)

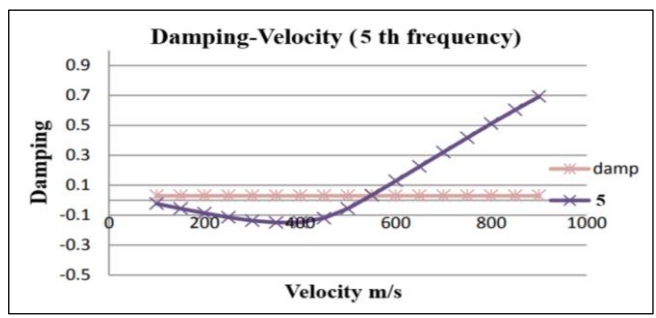

(b)

Figure 19: Damping-velocity curve

Figure 20 shows the normal modes that cause flutter, namely the 2nd bending mode at frequency 3 and the first torsion mode at frequency 7. Other

normal modes and optimized natural frequencies are not shown in this paper.

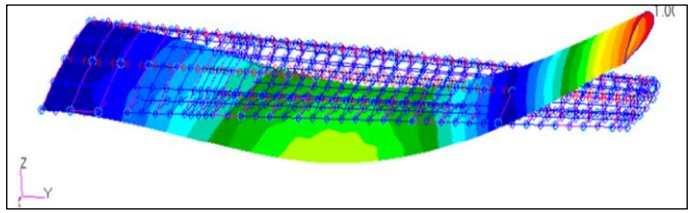

(a)

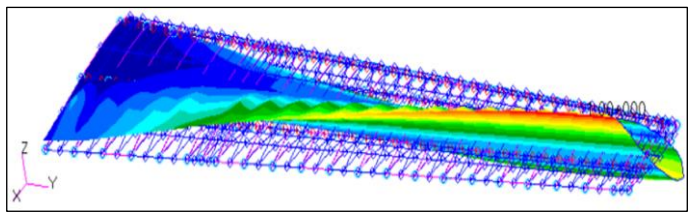

(b)

Figure 20: (a) 2nd bending mode, and (b) torsion mode

Comparison after and before optimization (flutter constraints)

Optimization using a flutter speed limit of 500 m/s has been carried out and resulted in a weight reduction of up to 80%; the weight of the structure, which was originally 482 kg, is now only 97 kg. Table 8 shows comparisons between before and after optimization. Before optimizing, the flutter speed was 860 m/s and then dropped to 550 m/s. At first, the first torsion mode occurred in the 4th mode, but after being optimized, the first torque mode shifted to the 5th frequency. The initial attenuation of -0.09 then becomes close to 0 at -2.00E-07. The first natural frequency drops from 10.94 Hz to 7.38 Hz.

Table 8: Comparison between before and after optimization

Flutter Constraints	Before	After Optimization
Structure weight	482 kg	97 kg
Flutter Speed	860 m/s	550 m/s
Damping at 500 m/s	-0.09	-2.00E-7
Coupled modes	3rd and 4th	3rd and 5th
Minimum natural frequency	10.94 Hz	7.38 Hz

A final design that meets all constraints

After optimization with the limits of static stress, buckling factor, and flutter

speed, the most appropriate design that meets all these limitations is selected.

Structural weights and final design variables

Figure 21 shows the comparison of the weight of the optimization results with the limitations that have been carried out. From the Figure, the structure with buckling constraints has the largest total weight compared to the others, meaning that if a configuration based on flutter speed or static stress is used, the structure is not safe from the buckling factor limit. Therefore, the final configuration taken is the configuration after optimization with a buckling factor limit and a total structure weight of 484 kg.

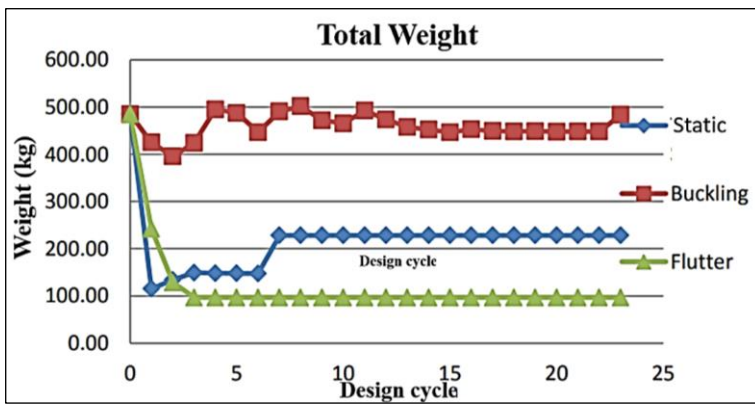

Figure 21: The weight comparison of the wing structure of each Constraint

Table 9 provides a detailed comparison of the thickness of each component before and after the optimization process. This table allows for a comprehensive evaluation of the changes in component thickness resulting from the optimization efforts. By analyzing the values presented in the table, one can gain valuable insights into the impact of the optimization on the structural dimensions of the components.

This paper is compared to previous works by Hadi et al. [8]-[9], and Kusni et al. [15], which also investigate the optimization of aircraft wing structures using a finite element model and composite materials under multiple constraints. However, there are notable distinctions between the two studies. Bambang's research focuses on UAV wings, while our study concentrates on wings designed for a 19-passenger aircraft.

Hadi et al. [8]-[9] present only the structural thickness, while our paper provides comprehensive information on the thickness of each composite fiber direction in all wing components. Additionally, our study includes a detailed account of the thickness variations throughout the optimization process. Furthermore, our paper exhibits a more extensive exploration of composite

fiber orientations.

Table 9: Initial and final composite configuration of each component

	Fiber	Skin		Rib		Front Spar		Rear Spar	
	Orientation	Initial	Final	Initial	Final	Initial	Final	Initial	Final
	0°	8	12			8	2	8	3
	45°	8	7			8	3	8	3
0	**135°**	8	7	-		8	3	8	3
	90°	8	7			8	3	8	2
	Total	**64**	**66**			**64**	**22**	**64**	**22**
	0°	7	9	4	2	7	2	7	1
	45°	7	10	4	2	7	3	7	3
1	135°	7	10	4	2	7	3	7	3
	90°	7	10	4	1	7	1	7	2
	Total	**56**	**78**	**32**	**14**	**56**	**18**	**56**	**18**
	0°	6	11	4	1	6	1	6	3
	45°	6	5	4	2	6	3	6	3
2	135°	6	5	4	2	6	3	6	3
	90°	6	8	4	1	6	3	6	3
	Total	**48**	**58**	**32**	**12**	**48**	**20**	**48**	**22**
	0°	6	3	3	2	4	2	4	2
	45°	6	7	3	2	4	2	4	2
3	135°	6	7	3	2	4	2	4	2
	90°	6	10	3	2	4	2	4	2
	Total	**48**	**54**	**24**	**16**	**32**	**16**	**32**	**16**
	0°	5	4	3	2	3	2	3	2
	45°	5	4	3	2	3	2	3	2
4	135°	5	4	3	2	3	2	3	2
	90°	5	9	3	2	3	1	3	2
	Total	**40**	**40**	**24**	**16**	**24**	**14**	**24**	**14**
	0°	4	3	2	2	2	2	2	2
	45°	4	3	2	2	2	2	2	2
5	135°	4	3	2	2	2	2	2	2
	90°	4	3	2	1	2	1	2	2
	Total	**32**	**24**	**16**	**14**	**16**	**14**	**16**	**16**
	0°	2	1	1	1	1	2	1	2
	45°	2	2	1	2	1	2	1	2
	135°	2	2	1	2	1	2	1	2
	90°	2	2	1	2	1	2	1	1
	Total	**16**	**14**	**8**	**14**	**8**	**16**	**8**	**14**

Overall, our research offers a more in-depth analysis of the wing structure, encompassing diverse constraints and providing valuable insights

into the optimization process specifically tailored for passenger aircraft wings.

Conclusions

The study aimed to optimize a wing structure to meet the Tsai-Hill failure criteria and prevent flutter. The initial structure was safe from buckling but still susceptible to buckling. After optimization, the structure's weight decreased by 53%, approaching a Tsai-Hill failure index closer to 1. The buckling factor, which previously did not meet safety criteria, is now within safe limits. The wing structure was found to be safe from flutter, even with a thin thickness. Optimization with flutter speed limitations resulted in reduced structure weight and improved flutter speed performance. The final configuration selected satisfies all set constraints, including static, buckling, and flutter. The optimization with a buckling factor constraint produced the greatest weight configuration, meeting all safety requirements.The initial wing structure before optimization met the Tsai-Hill failure criteria and was safe from flutter. However, it was still susceptible to buckling. After optimization, significant improvements were achieved in weight reduction and meeting the set constraints.

Contributions of Authors

The authors confirm the equal contribution in each part of this work. All authors reviewed and approved the final version of this work.

Acknowledgment

This paper was supported by the Scholarship Fund of P3MI, Faculty of Mechanical and Aerospace Engineering, ITB, Indonesia, from 1 August 2020 to 30 July 2023 (No. 516/IT1.B05/KP/2021).

References

[1] G. N. Vanderplaats “Structural optimization - Past, present, and future,” *AIAA Journal*, vol. 20, pp. 992-1000, 1981.

[2] R. Ganguli, “Optimal design of composite structures: A historical review,” *Journal of the Indian Institute of Science*, vol. 93, no. 4, pp. 557-570, 2013.

[3] N. Khot, V. Venkayya, C. Johnson and V. Tischler, “Optimization of

Fiber Reinforced Composite Structures," *International Journal of Solids and Structures*, vol. 9, pp. 1225-1236, 1973.
[4] J. H. Starnes and R. T. Haftka, "Preliminary Design of Composite Wings for Buckling, Strength, and Displacement Constraints," *Journal of Aircraft*, vol. 16, pp. 564-570, 1979.
[5] T.A. Weisshaar, "Aeroelastic Tailoring of Forward Swept Composite Wing," *Journal of Aircraft*, vol. 18, pp. 669-676, 1981.
[6] M. H. Shirk and T. J. Hertz, "Aeroelastic tailoring - Theory, practice, and promise," *Journal of Aircraft*, vol. 23, pp. 6-18, 1986.
[7] F. Eastep, V. Tischler, V. Venkayya and N. Khot, "Aeroelastic Tailoring of Composite Structures," *Journal of Aircraft*, vol. 36, no. 6, pp. 1041-1047, 1999.
[8] B. K. Hadi, M.A. Ghofur, and I. Permana, "The design of a high aspect ratio HALE aircraft composite wing. Part I: Static Strength Analysis." *Journal of Mechanical Engineering*, vol 12, pp. 1-11, 2015
[9] B. K. Hadi, M.A. Ghofur, and I. Permana, "The design of a high aspect ratio HALE aircraft composite wing. Part II: Buckling and flutter speed analysis", *Journal of Mechanical Engineering*, vol 12, pp. 13-26, 2015
[10] Zexi, Zhiqiang, Rainer, Xiaozhe "Aeroelastic and local buckling optimization of a variable-angle-tow composite wing- Box strcutures", *Composite Structures*, vol. 258, pp. 1-18, 2020.
[11] R. Feil, T. Pflumm, P. Bortolotti, M. Morandini, "A cross-sectional aeroelastic analysis and structural optimization tool for slender composite structures" *Composite Structures*, vol. 253, pp. 1-11, 2020.
[12] W. Yang, Z. Yue, L. Li, and P. Wang, "Aircraft wing structural design optimization based on automated finite element modeling and ground structure approach," *Journal Engineering Optimization*, vol. 48, no. 1, pp. 94–114, 2016.
[13] Eirikur, Cristina, Christopher, Carlos, Joaquim, Bogdan "Flutter and post-flutter constraints in aircraft design optimization", *Progress in Aerospace Sciences*, vol. 109, pp. 1-28, 2019.
[14] Claudia, Miguel, Eric, Sebastien, Guilhem, Annie "Comparison of low, medium and high fidelity numerical methods for unsteady aerodynamics and nonlinear aeroelasticity," *Journal of Fluids and Structure*, vol. 91, pp. 1-12, 2019.
[15] G. N. Vanderplaats, "Structural Optimization - Past, Present, and Future," *AIAA Journal*, pp. 992-1000, 1981.
[16] M. Kusni, M. Widiramdhani, and B. K. Hadi, "Sensitivity study and structural optimization of wing with maximum-stress and flutter constraint," in *IOP Conference Series Materials Science and Engineering*, vol. 1173, no. 1, pp. 1-10, 2021.
[17] Eirikur, Cristina, Christopher, Carlos, Joaquim, Bogdan "Flutter and post-flutter constraints in aircraft design optimization" *Journal Progress in Aerospace Sciences*, vol. 109, pp. 1-77, 2019

[18] G. Soremekun, Z. Gurdal, R. Haftka, and L. Watson, "Composite laminate design optimization by genetic algorithm with generalized elitist selection", *Computers & Structures*, vol. 79, pp. 131-143, 2001.
[19] W. Mark and R. E. Smith, "A technique for multiobjective optimisation of laminated composite structures using genetic algorithms and finite element analysis", *Composite Structures*, vol. 62, pp. 123-128, 2003.
[20] N. G. Naik, G. S., and R. Ganguli, "Design optimization of composites using genetic algorithms and failure mechanism based failure criterion", *Composite Structures*, vol. 83, pp. 354-367, 2008.
[21] M. K. Apalak, D. Karaboga, Akay and Bahriiye, "The artificial bee colony algorithm in layer optimization for the maximum fundamental frequency of symmetrical laminated composites plates", *Engineering Optimization*, vol. 46, no. 3, pp. 1-18, 2014.
[22] I. M. Daniel and O. Ishai, Engineering Mechanics of Composite Materials, New York: Oxford University Press, Inc., 2006.